TÜBİTAK

Turkish Journal of Physics

http://journals.tubitak.gov.tr/physics/

Research Article

Turk J Phys
(2016) 40: 12 – 23

doi:10.3906/fiz-1507-25

# A study on $^{7}$Li + $^{120}$Sn quasi-elastic scattering

**Murat AYGÜN**[1,*], **Zeynep AYGÜN**[2]
[1]Department of Physics, Faculty of Science, Bitlis Eren University, Bitlis, Turkey
[2]Vocational School of Technical Sciences, Bitlis Eren University, Bitlis, Turkey

**Received:** 20.07.2015 • **Accepted/Published Online:** 10.11.2015 • **Final Version:** 12.02.2016

**Abstract:** In the present study, we reexamine quasi-elastic scattering of $^{7}$Li by $^{120}$Sn at incident energies $E_{Lab}$ = 19.5, 20.5, and 25.0 MeV. The theoretical results are obtained by using both a phenomenological model and double-folding model (DFM) within the framework of an optical model. We also investigate the role of the surface potential, which is connected to direct reactions. The agreement between the phenomenological model and the DFM is shown in comparison to each other in connection with the experimental data. This comparison provides information about the similarities and the differences between the models used during the calculations.

**Key words:** Optical model, double-folding model, elastic scattering, quasi-elastic scattering

## 1. Introduction

The scattering of stable isotopes of lithium from different target nuclei at various energies has been studied largely over the past few decades [1–5]. $^{7}$Li, which has gained attention in the field of nuclear physics, is one of these nuclei. Many experimental and theoretical studies have been carried out. In these studies, various interactions such as elastic scattering, inelastic scattering, fusion reactions, and transfer reactions have been measured and investigated [6–23]. However, we need further theoretical work in order to better understand the experimental data of the reactions concerning $^{7}$Li because there are still ambiguities in the way that $^{7}$Li–nucleus interactions are understood. For example, in the studies performed by using the double-folding model (DFM) based on the optical model (OM), it was found that renormalization was required [24–26] due to the importance of the breakup effect [27]. Hence, it can be interesting to investigate the renormalization of double-folded potentials for the different scattering data. As a result of this, we consider that it would be useful for the problem of renormalization of $^{7}$Li with various target nuclei.

Recently, Sousa et al. [28] measured quasi-elastic scattering data of a $^{7}$Li + $^{120}$Sn system at incident energies $E_{Lab}$ = 19.5, 20.5, and 25.0 MeV. They also investigated the density distribution of the $^{7}$Li light nucleus using the São Paulo potential within the framework of the OM. They reported that the disagreement observed between theoretical and experimental results obtained by means of $^{7}$Li nucleon density was due to the inclusion of additional reaction processes in OM calculations. The quasi-elastic scattering was assumed to be the sum of elastic and inelastic scattering due to the limited energy resolution in the experimental measurements. Various approaches are used when analyzing scattering data. The OM is one of the most preferred models when explaining elastic scattering angular distribution. The DFM, which uses the density distributions of both the projectile and the target, is also known to be very important for these studies.

*Correspondence: maygun@beu.edu.tr

In this work, we reanalyze the quasi-elastic scattering angular distributions of the $^{7}$Li + $^{120}$Sn system at $E_{Lab}$ = 19.5, 20.5, and 25.0 MeV by using both a phenomenological model and a DFM based on an OM. To obtain the real optical potential we use both the phenomenological Woods–Saxon (WS) model and the DFM. The imaginary part of the potential is taken as a phenomenological WS model. Our purpose in this analysis is to investigate the ability of the volume and surface potentials to reproduce the quasi-elastic $^{7}$Li + $^{120}$Sn scattering data. For this purpose, the imaginary part of the optical potential is divided into two parts, consisting of the volume potential and the surface potential. In addition, we aim to investigate the effect of surface potential on the normalization of the DFM. All obtained results are compared with the experimental data. Thus, the similarities and differences between the models used in obtaining the theoretical results are discussed.

In the present study, Section 2 is devoted to the different approaches used in the theoretical analyses intended for the interpretation of the experimental data. Section 3 summarizes the work and discusses the conclusions.

## 2. Theoretical analysis

In this section, we examine the scattering data of $^{7}$Li on $^{120}$Sn target nuclei with the aid of the phenomenological model and the DFM at different energies. In theoretical calculations, it is assumed that the total effective potential contains nuclear and Coulomb potentials. Thus, it is given as

$$V_{total}(r) = V(r) + iW(r) + V_{Coulomb}(r). \tag{1}$$

The Coulomb potential is given by [29]

$$V_{\text{Coulomb}}(r) = \frac{1}{4\pi\varepsilon_0}\frac{Z_P Z_T e^2}{r}, \qquad r \geq R_C \tag{2}$$

$$= \frac{1}{4\pi\varepsilon_0}\frac{Z_P Z_T e^2}{2R_C}(3 - \frac{r^2}{R_C^2}), \qquad r \leq R_C \tag{3}$$

where $R_C$ is the Coulomb radius, taken as $1.25(A_P^{1/3} + A_T^{1/3})$ fm in the calculations, and $Z_P$ and $Z_T$ denote the charges of projectile $P$ and target nuclei $T$, respectively. For the theoretical calculations of both the phenomenological model and the DFM, the code FRESCO [30] has been used. FRESCO, which is a general-purpose reaction code, is used for determining the parameters of the OM to fit the experimental data for any investigated nuclear reaction [31].

### 2.1. Phenomenological analysis

In phenomenological analysis, the real part of the nuclear potential is accepted to be the WS type as represented in the following form:

$$V_{real}(r) = -V_0 f(r, R_i, a_i), \tag{4}$$

$$f(r, R_i, a_i) = \frac{1}{1 + exp(\frac{r - R_i}{a_i})}, \tag{5}$$

where $R_i = r_i\,(A_P^{1/3} + A_T^{1/3})$ $(i = V$ or $W)$, and $A_P$ and $A_T$ are the masses of the projectile and target nuclei, respectively.

The imaginary potential is taken as WS volume potential in the following form:

$$V_{imaginary}(r) = -W_0 f(r, R_i, a_i). \tag{6}$$

Thus, the total nuclear potential is written as

$$V_{Nuclear}(r) = -\frac{V_0}{1 + exp(\frac{r-Rv}{a_v})} - i\frac{W_0}{1 + exp(\frac{r-R_w}{a_w})}. \tag{7}$$

We investigated the agreement between the theoretical results and the experimental data of $^{7}$Li + $^{120}$Sn by searching for the $V_0$ (the depth of the real part), $r_v$ (the radius of the real part), $a_v$ (the diffuseness of the real part), $W_0$ (the depth of the imaginary part), $r_w$ (the radius of the imaginary part), and $a_w$ (the diffuseness of the imaginary part) parameters of the real and the imaginary parts of optical potential. We simultaneously performed the OM calculations for various values of the parameters $r_v$ and $r_w$ in the range of 0.9 to 1.4 fm in order to reduce the number of OM parameters. After a comparative analysis of these results together with the experimental data, we observed that $r_v = 1.180$ fm and $r_w = 1.386$ fm. The $a_v$ and $a_w$ values of the optical potential were varied within the range of 0.4 to 1.0 fm at fixed radii and were taken as $a_v = a_w = 0.515$ fm for each energy. Finally, the fitting procedure was completed by changing the depths of real and imaginary potential of OM for different incident energies. All the values of the parameters used when obtaining theoretical results are shown in Table 1. The results given in comparison with the experimental data in Figures 1–3 are not in very good agreement and miss some experimental data. This result is expected because of the fact that OM calculation alone cannot define the quasi-elastic scattering data, which include both elastic and inelastic effect. We looked for better results from the OM for explaining the experimental data in order to advance the theoretical results of our study. With this goal, we once again conducted the theoretical calculations for the imaginary potential, accepting it as the sum of WS volume and the surface potential as seen in the following form:

$$V_{imaginary}(r) = -W_v f(r, R_i, a_i) + 4W_s a_s \frac{df(r, R_s, a_s)}{dr}. \tag{8}$$

For determining the optical parameters of this case, we only changed the surface potential parameters while the WS volume parameters were accepted to be the same as in the previous calculations. It is only possible to observe the role of the surface potential when the OM parameters of the volume potential are not changed. We provide the values of all the parameters in Table 1. We also compared the OM results together with and without the surface potential as well as the experimental data, as shown in Figures 1–3. In general, we observed that the theoretical results of the OM with the WS volume and the surface potential were better than the results with only the WS volume potential.

### 2.2. Double-folding model analysis

Here, we determine the real part of the nuclear potential the help of the DFM, which uses the nuclear matter distributions of both the projectile and the target nuclei together with an effective nucleon–nucleon interaction potential ($\nu_{NN}$). The double-folding potential is given as

$$V_{\text{doublefolding}}(r) = \int dr_1 \int dr_2 \rho_P(r_1)\rho_T(r_2)v_{NN}(r_{12}), \tag{9}$$

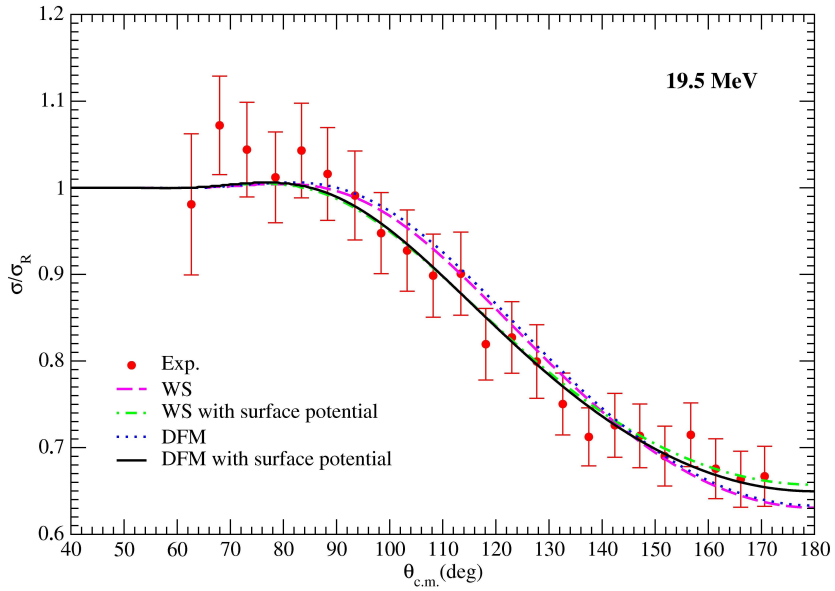


**Figure 1.** The elastic scattering angular distributions for $^{7}$Li + $^{120}$Sn at $E_{Lab}$ = 19.5 MeV. The dashed line shows phenomenological results with WS type potential, dashed-dotted line shows phenomenological results with WS plus surface potential, dotted line shows DFM results, and solid line shows DFM results with surface potential. The circles show the experimental data, which were taken from [28].

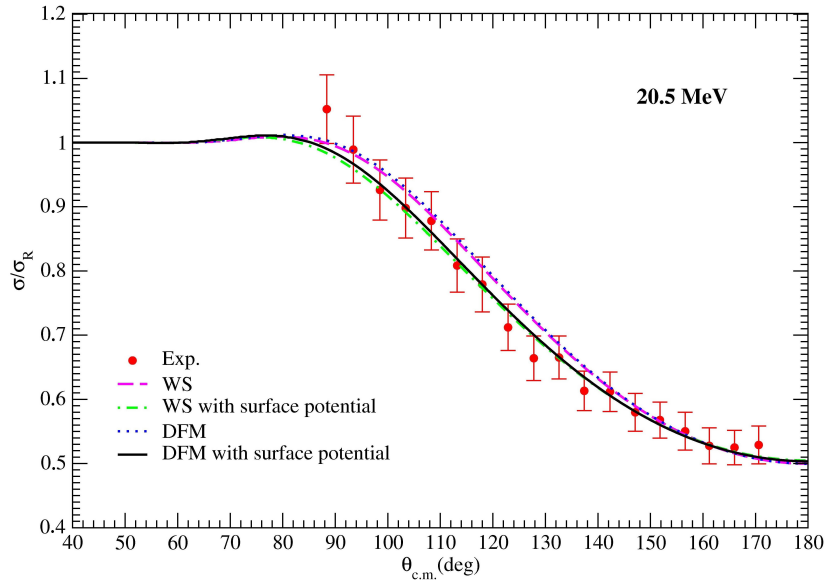


**Figure 2.** The elastic scattering angular distributions for $^{7}$Li + $^{120}$Sn at $E_{Lab}$ = 20.5 MeV. The dashed line shows phenomenological results with WS type potential, dashed-dotted line shows phenomenological results with WS plus surface potential, dotted line shows DFM results, and solid line shows DFM results with surface potential. The circles show the experimental data, which were taken from [28].

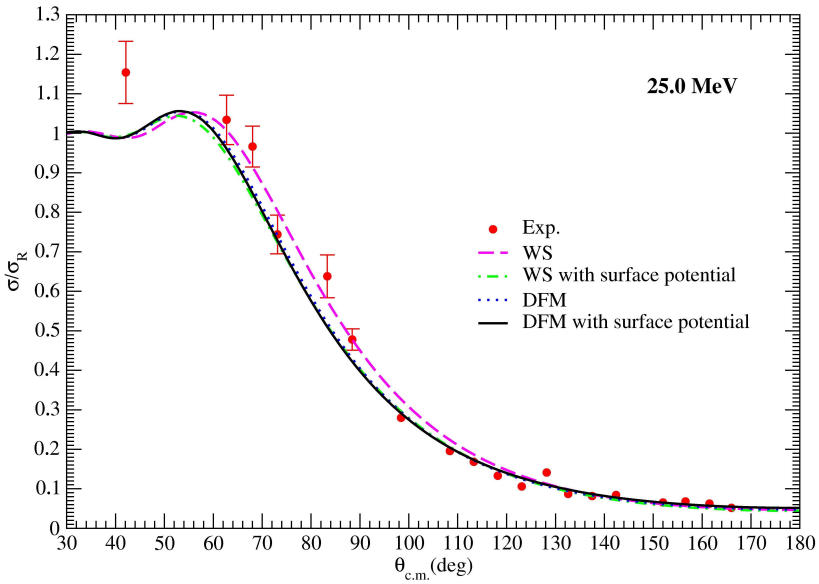


**Figure 3.** The elastic scattering angular distributions for $^{7}$Li + $^{120}$Sn at $E_{Lab}$ = 25.0 MeV. The dashed line shows phenomenological results with WS type potential, dashed-dotted line shows phenomenological results with WS plus surface potential, dotted line shows DFM results, and solid line shows DFM results with surface potential. The circles show the experimental data, which were taken from [28].

**Table 1.** The optical model parameters used in phenomenological model analysis of $^{7}$Li + $^{120}$Sn reaction.

| $E_{Lab}$ MeV | Potential type | $V_0$ MeV | $r_v$ fm | $a_v$ fm | $W_0$ MeV | $r_w$ fm | $a_w$ fm | $W_s$ MeV | $r_s$ fm | $a_s$ fm | $J_v$ MeV fm$^3$ | $J_w$ MeV fm$^3$ | $\chi^2$ – | $\sigma$ mb |
|---|---|---|---|---|---|---|---|---|---|---|---|---|---|---|
| 19.5 | WS | 160.0 | 1.18 | 0.515 | 18.4 | 1.386 | 0.515 | - | - | - | 437.4 | 80.6 | 0.62 | 119.0 |
| | WS+surface | 160.0 | 1.18 | 0.515 | 18.4 | 1.386 | 0.515 | 9.4 | 1.446 | 0.300 | 437.4 | 97.2 | 0.44 | 133.5 |
| 20.5 | WS | 117.0 | 1.18 | 0.515 | 8.95 | 1.386 | 0.515 | - | - | - | 319.8 | 39.2 | 1.00 | 156.2 |
| | WS+surface | 117.0 | 1.18 | 0.515 | 8.95 | 1.386 | 0.515 | 7.0 | 1.336 | 0.420 | 319.8 | 54.0 | 0.58 | 183.4 |
| 25.0 | WS | 103.0 | 1.18 | 0.515 | 9.10 | 1.386 | 0.515 | - | - | - | 281.6 | 39.9 | 6.00 | 701.1 |
| | WS+surface | 103.0 | 1.18 | 0.515 | 9.10 | 1.386 | 0.515 | 1.5 | 1.443 | 0.485 | 281.6 | 44.2 | 8.02 | 804.0 |

where $\rho_P$ ($r_1$) and $\rho_T$ ($r_2$) are the nuclear matter density of projectile and target nuclei, respectively. When obtaining the folding potential, the ground state density distribution of the $^{7}$Li projectile has been taken as shown in the following form [32]:

$$\rho(r_1) = 0.1387(1 + 0.1673r_1^2)\exp(-0.3341r_1^2). \tag{10}$$

In Figure 4, this density distribution is plotted at both logarithmic and linear scale. The density distribution of the $^{120}$Sn target nucleus was taken from RIPL-3 [33]. We have chosen the M3Y (Michigan 3 Yukawa) nucleon–nucleon realistic interaction as shown by

$$v_{NN}(r) = 7999\frac{exp(-4r)}{4r} - 2134\frac{exp(-2.5r)}{2.5r} - 276\,[1 - 0.005\,E_{Lab}/A_P]\,\delta(r), \tag{11}$$

where exchange (the last term in equation) has a linear energy dependence.

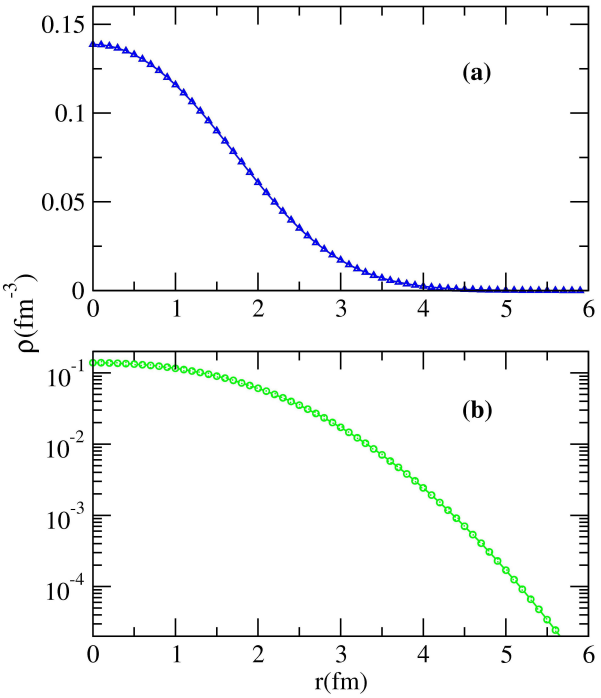


**Figure 4.** The density distribution of the $^{7}$Li nucleus plotted as both linear scale (top) and logarithmic (bottom).

To obtain the imaginary part of the nuclear potential, the WS potential in the following form has been used:

$$W(r) = -W_0 f(r, R_w, a_w), \tag{12}$$

where

$$f(r, R_w, a_w) = \frac{1}{1 + exp(\frac{r - R_w}{a_w})}. \tag{13}$$

The compliance between the theoretical results data and experimental data was investigated by changing $W_0$, $r_w$, and $a_w$ values of the imaginary potential. After the OM calculations were carried out for different values of $r_w$ in steps from 0.1 to 0.001 fm between 0.9 fm and 1.4 fm at each incident energy, we took 1.396 fm as the value of $r_w$. The $a_w$ value of the potential was varied in steps from 0.1 to 0.001 fm between 0.4 fm and 1.0 fm at a fixed radius and was taken as 0.490 fm. Finally, the fitting procedure of the experimental data was completed by changing the depth of the imaginary potential. The theoretical results obtained for the parameters given in Table 2 are shown in comparison with the experimental data in Figures 1–3. The results are not in good consistency with the data. To overcome this situation, we added a surface potential to the WS volume potential used in the OM calculations and searched for the best parameters to fit to the experimental data, which are given in Table 2. We show the results of other theoretical models as well as the experimental data in Figures 1–3 as a comparison. In Figure 1 the results with the surface potential appear to be successful in the description of the experimental data. On the other hand, the results of WS and bare folding potentials are quite inadequate in the explanation of both backward and forward angles of the experimental data. If we investigate Figure 2, we observe similar results at 19.5 MeV. While the surface potentials are successful in explaining experimental data, WS and bare folding potentials are not in good agreement with the experimental data. However, the harmony with the experimental data of WS and bare folding potentials increases in forward angles (about from 140° to

172°). It can be seen from Figure 3 that the results with the surface and bare folding potentials, which exhibit very similar behaviors, are more consistent with the experimental data than the results with WS potential. On the other hand, the results with WS potential are better than the results with the surface and bare folding potentials in backward angles. However, all the theoretical results have been seen to be very coherent with each other in forward angles (from about 125° to 180°). We observed that the addition of the surface potential provided results in good agreement with the experimental data. If our results are compared with the results of Sousa et al. [28], it can be seen that our theoretical results are better than their results. As a result of this, the addition of the surface potential to the calculations is incontrovertible, because this potential includes the role of other interactions such as direct reactions. This situation can be seen from the results with the surface potential of both the phenomenological model and the DFM.

**Table 2.** The optical model parameters used in double-folding model analysis of $^{7}$Li + $^{120}$Sn reaction.

| $E_{Lab}$ MeV | Potential type | $N_R$ | $W_0$ MeV | $r_w$ fm | $a_w$ fm | $W_s$ MeV | $r_s$ fm | $a_s$ fm | $J_v$ MeV fm$^3$ | $J_w$ MeV fm$^3$ | $\chi^2$ – | $\sigma$ mb |
|---|---|---|---|---|---|---|---|---|---|---|---|---|
| 19.5 | WS | 1.05 | 18.0 | 1.396 | 0.490 | - | - | - | 433.5 | 80.4 | 0.60 | 111.6 |
| | WS+surface | 1.00 | 18.0 | 1.396 | 0.490 | 17.0 | 1.396 | 0.342 | 412.8 | 112.3 | 0.38 | 132.4 |
| 20.5 | WS | 0.78 | 9.10 | 1.396 | 0.490 | - | - | - | 321.9 | 40.6 | 0.94 | 149.7 |
| | WS+surface | 0.84 | 9.10 | 1.396 | 0.490 | 8.0 | 1.326 | 0.400 | 346.6 | 56.5 | 0.46 | 174.1 |
| 25.0 | WS | 0.90 | 15.00 | 1.396 | 0.490 | - | - | - | 370.6 | 67.0 | 4.14 | 769.0 |
| | WS+surface | 1.00 | 15.00 | 1.396 | 0.490 | 4.5 | 1.286 | 0.400 | 345.9 | 75.4 | 4.92 | 781.6 |

In double-folding calculations, a normalization factor ($N_R$), which was changed to obtain good agreement results with the experimental data, was used. The value $N_R = 1.0$ shows the success of the model used in the calculations [26]. If the deflection from unity for $N_R$ is required, the model would need the corrections. This state is attributed to strangeness and uncertainties in the data, or to uncertainties in the fitting procedures applied or to uncertainties in the densities used in the calculations [26]. Vineyard et al. [32] reported that the normalization value of $^{7}$Li was found as $N_R \approx 0.7$ in $^{7}$Li + $^{12}$C calculations. They put forward the projectile breakup effects as the reason for this. With this in mind, if we examine the change of the normalization constant in our DFM calculations, we would be able to observe that the DFM results without surface potential are coherent with earlier results. In this respect, $N_R$ took the values of 0.78, 0.90, and 1.05 in our study, but the harmony between the theoretical results and the experimental data was not very good. As seen in Figure 5, when we examined DFM results with the surface potential, we noticed that the $N_R$ value, compared to the default value $N_R = 1.0$ [26], gets 8% better when compared with previous DFM results. This consistency of the theoretical results with the experimental data is seen in Figures 1–3.

We show the cross-sections of all the interactions in comparison to each energy in Figure 6. We observed that the cross-sections exhibit similar behaviors with the increase in energy. The cross-sections for both sets of OM and DFM calculations show a continuous increase. It can be said that the similar behavior of the cross-sections is an indication of the compatibility of the used models.

The harmony between theoretical results and experimental data was determined by the help of the usual reduced $\chi^2$ as given below:

$$\chi^2 = \frac{1}{N_\sigma - N_p} \sum_{i=1}^{N_\sigma} \frac{\left(\sigma_{theo} - \sigma_{\exp}\right)^2}{\left(\Delta\sigma_{\exp}\right)^2}, \tag{14}$$

where $\sigma_{theo}$ is the theoretical cross-section obtained by searching the potential parameters, $\sigma_{exp}$ is the experimental cross-section, $\Delta\sigma_{exp}$ is the error variation of the experimental cross-section, $N_\sigma$ is the number of

the experimental points, and $N_p$ is the number of searched parameters in fitting [34]. It has been expressed in previous studies that the $\chi^2$ value, which has a minimum, is not always an indication of a better visual result.

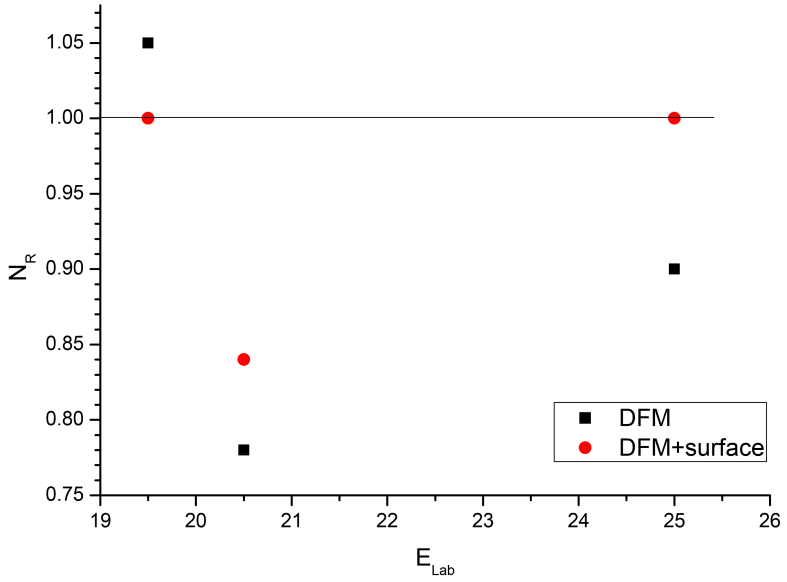


**Figure 5.** The normalization constants as a function of energy. The filled squares show DFM results and the filled circles show DFM results with surface potential. The solid line, which indicates $N_R = 1$, is to guide the eye.

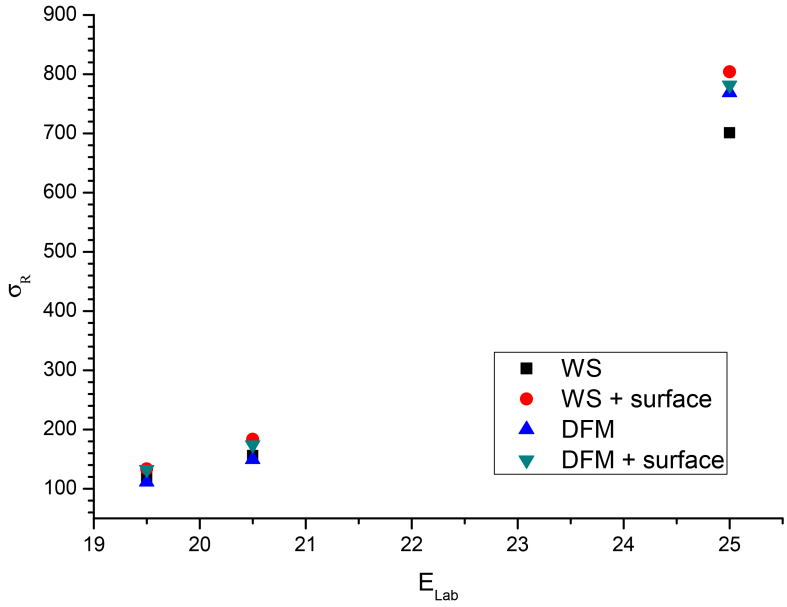


**Figure 6.** The cross-sections obtained by phenomenological model and DFM of $^{7}$Li + $^{120}$Sn system as a function of energy, which are given comparatively. The filled squares show WS results, the filled circles show WS results with surface potential, the filled upward triangle shows DFM results, and the filled downward triangle shows DFM results with surface potential.

Sometimes, determining how compatible the investigated fit is by eye may be more efficient than the $\chi^2$ value [29,35,36]. While the $\chi^2$ values were calculated, first, the percentage errors for points of the experimental data of each energy were determined. Then the average experimental percentage errors over these error values were calculated around 5.25% for 19.5 MeV, 4.90% for 20.5 MeV, and 6.5% for 25 MeV. Thus, we calculated the $\chi^2$ values according to these experimental percentage error values for each model and energy. We provide the $\chi^2$ values for all the interactions in Tables 1 and 2. We noticed that the $\chi^2$ values of the theoretical results were very small in general. The smallest $\chi^2$ values were obtained mostly in the surface potential case of both the phenomenological model and the DFM, which are seen in Figures 1–3. One should also point out that while the $N_R$ values of the DFM with surface potential are around 1.0, the $N_R$ values of the DFM decreases from 1.05 to 0.78. This indicates that the DFM with surface potential provides more reasonable results than the DFM.

In the present work, we have calculated the volume integrals of both the real part ( $J_v$) and the imaginary part ( $J_w$) of the optical potential. It is known that the volume integrals show similar behaviors for good fits of the optical potentials with different parameters [37]. The formulas used in this context were

$$J_v(E) = \frac{4\pi}{A_P A_T} \int V(r,E) r^2 dr \tag{15}$$

and

$$J_w(E) = \frac{4\pi}{A_P A_T} \int W(r,E) r^2 dr. \tag{16}$$

The $J_v$ and $J_w$ values obtained from each model investigated are given in Tables 1 and 2 and are plotted comparatively in Figures 7 and 8. Both the $J_v$ and $J_w$ values of the phenomenological model with and without surface potential decrease with the increasing of the incident energy. In the DFM results without surface potential, the $J_w$ values accompany a rapid change when the $J_v$ values also display a rapid change. However, the $J_v$ values of the DFM with surface potential decrease with the energy while the $J_w$ value displays a rapid change at 20.5 MeV. We should point out that the systematics of the energy dependence of the OM potential for $^7$Li scattering could not be shown in a precise way. With this goal, Deshmukh et al. [37] measured the elastic scattering data of $^7$Li scattered from $^{116}$Sn at various incident energies and analyzed the experimental data theoretically. They reported that the $^7$Li + $^{116}$Sn system at energies around and below the Coulomb barrier showed the absence of the threshold anomaly because of becoming energy-independent of real and imaginary parts of the optical potential. However, we cannot exactly say whether there is a threshold anomaly for the $^7$Li + $^{120}$Sn system investigated in our work. For this, more experimental data are needed, which would allow us to adequately explain the threshold anomaly.

## 3. Summary and conclusions

In the present work, we have analyzed quasi-elastic scattering data of the $^7$Li + $^{120}$Sn system at incident energies $E_{Lab}$ = 19.5, 20.5, and 25.0 MeV. We have used phenomenological and double-folding potential in calculations. We have observed that the theoretical results for both phenomenological (with WS volume potential) and DFM are not in good agreement with the experimental data. The volume imaginary potential of the optical potential is thought to be responsible for absorption because of the inelastic scattering, transfer, breakup, and fusion that occurred in nuclear interactions. Therefore, we have divided the imaginary part of the optical potential into two parts, which consisted of the volume potential and the surface potential. When we added the surface potential to

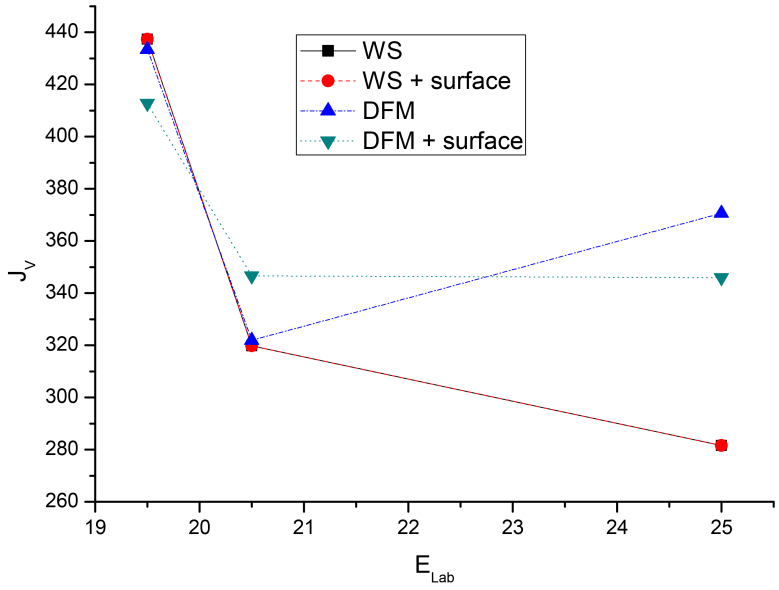


**Figure 7.** The change with the energy of the volume integral of the real part of the nuclear potential used in the calculations of the OM and DFM. The solid line shows phenomenological results of WS type potential with and without surface potential, the dashed line shows DFM results, and the dashed-dotted line shows DFM results with surface potential. The curves are to guide the eye.

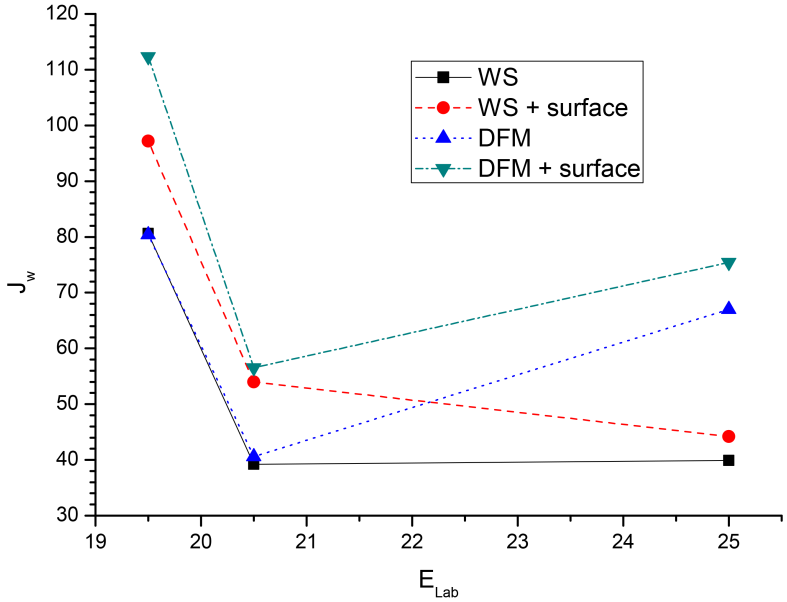


**Figure 8.** The change with the energy of the volume integral of the imaginary part of the nuclear potential used in the calculations of the OM and DFM. The solid line shows phenomenological results with WS type potential, the dashed line shows phenomenological results with WS plus surface potential, the dotted line shows DFM results, and the dashed-dotted line shows DFM results with surface potential. The curves are to guide the eye.

the calculations performed for these theoretical models, we observed an improvement in the theoretical results. This might be a result of the surface potential from inelastic or reaction processes that occurred in the surface of the nucleus. Additionally, the scattering at low energy does not show much sensitivity to the interior while the projectile with high energy penetrates the interior. Moreover, the $N_R$ values with the surface potential got better by about 8% according to the $N_R$ values obtained without the surface potential. Therefore, we concluded that the surface potential includes the effect of the direct reactions and this provides an improvement in theoretical results. We can say that the surface potential needs to be considered when explaining the quasi-elastic scattering data of the $^{7}$Li projectile scattered from the $^{120}$Sn target nucleus. Finally, we have given the $\chi^2$ values and the volume integrals of the real and the imaginary potential of the phenomenological model and the DFM in tables and have displayed all the results of the calculations in figures.

## References


[1] Bassani, G.; Saunier, N.; Traore, B. M. *Nucl. Phys. A* **1972**, *189*, 353–367.

[2] Chua, L. T.; Becchetti, F. D.; Jänecke, J.; Milder, F. L. *Nucl. Phys. A* **1976**, *273*, 243–252.

[3] Keeley, N.; Bennett, S. J.; Clarke, N. M.; Fulton, B. R.; Tungate, G.; Drumm, P. V.; Nagarajan, M. A.; Lilley, J. S. *Nucl. Phys. A* **1994**, *571*, 326–336.

[4] Poling, J. E.; Norbeck, E .; Carlson, R. R. *Phys. Rev. C* **1976**, *13*, 648.

[5] Aygun, M. *Eur. Phys. J. A* **2012**, *48*, 145.

[6] Fatemian, M.; Buck, B. *Phys. Letts. B* **1989**, *231*, 25–27.

[7] Cutler, R. I.; Nadworny, M. J.; Kemper, K. W. *Phys. Rev. C* **1977**, *15*, 1318.

[8] Pinilla, E. C.; Descouvemont, P. *Phys. Rev. C* **2014**, *89*, 054615.

[9] Freiesleben, H.; Rizzo, G. T.; Huizenga, J. R. *Phys. Rev. C* **1975**, *12*, 42.

[10] Potthast, K. W.; Brand, H.; Freiesleben, H.; Rosenthal, P.; Kamys, B.; Schieck, H. P. gen.; Sydow, L. *Nucl. Phys. A* **1997**, *614*, 95–111.

[11] Palshetkar, C. S.; Thakur, S.; V.; Shrivastava, A.; Dokania, N.; Singh, V.; Parkar, V. V.; Rout, P. C.; Palit, R.; Pillay, R. G. et al. *Phys. Rev. C* **2014**, *89*, 024607.

[12] Keeley, N.; Kemper, K. W.; Rusek, K. *Phys. Rev. C* **2001**, *65*, 014601.

[13] Moore, G. E.; Kemper, K. W.; Charlton, L. A. *Phys. Rev. C* **1975**, *11*, 1099.

[14] Lubian, J.; Correa, T.; Paes, B.; Figueira, J. M.; Abriola, D.; Fernández Niello, J. O.; Arazi, A.; Capurro, O. A.; Barbará, E. de.; Martí, G. V. et al. *Nucl. Phys. A* **2007**, *791*, 24–35.

[15] Potthast, K. W.; Freiesleben, H.; Rosenthal, P.; Kamys, B.; Rudy, Z.; Schieck, H. P. gen.; Sydow L. *Nucl. Phys. A* **1998**, *629*, 656–676.

[16] Rudchik, A. T.; Chercas, K. A.; Kemper, K. W.; Rudchik, A. A.; Kliczewski, S.; Koshchy, E. I.; Rusek, K.; Mezhevych, S. Yu.; Ponkratenko, O. A.; Pirnak, V. M. et al. *Nucl. Phys. A* **2014**, *927*, 209–219 .

[17] Descouvemont, P.; Hussein, M. S. *Phys. Rev. Letts.* **2013**, *111*, 082701.

[18] Davis, N. J.; Ward, R. P.; Rusek, K.; Clarke, N. M.; Tungate, G.; Griffith, J. A. R.; Hall, S. J.; Karban, O.; Martel-Bravo, I.; Nelson, J. M. et al. *Phys. Rev. C* **2004**, *69*, 064605.

[19] Kalita, K.; Verma, S.; Singh, R.; Das, J. J.; Jhingan, A.; Madhavan, N.; Nath, S.; Varughese, T.; Sugathan, P.; Parkar, V. V. et al. *Phys. Rev. C* **2006**, *73*, 024609.

[20] Martel, I.; Gómez-Camacho, J.; Blyth, C. O.; Clarke, N. M.; Dee, P. R.; Fulton, B. R.; Griffith, J. A. R.; Hall, S. J.; Keeley, N.; Tungate, G. et al. *Nucl. Phys. A* **1995**, *582*, 357–368.

[21] Al-Sa'ad, A. A. *Chinese J. Phys.* **2014**, *52*, 1218.

[22] Martel, I.; Gómez-Camacho, J.; Rusek, K.; Tungate, G. *Nucl. Phys. A* **1998**, *641*, 188–202.

[23] Cook, J.; Kemper, K. W.; Drumm, P. V.; Fifield, L. K.; Hotchkis, M. A. C.; Ophel, T. R.; Woods, C. L. *Phys. Rev. C* **1984**, *30*, 1538.

[24] Tungate, G. *J. Phys. G Nucl. Phys.* **1986**, *12*, 1001–1016.

[25] Martel, I.; Gómez-Camacho, J.; Rusek, K.; Tungate, G. *Nucl. Phys. A* **1996**, *605*, 417–431.

[26] Satchler, G. R.; Love, W. G. *Phys. Rep.* **1979**, *55*, 183–254.

[27] Nagarajan, M. A.; Thompson, J.; Johnson, R. C. *Nucl. Phys. A* **1982**, *385*, 525–536.

[28] Sousa, D. P.; Pereira, D.; Lubian, J.; Chamon, L. C.; Oliveira, J. R. B.; Rossi, E. S. Jr.; Silva, C. P.; de Faria, P. N.; Guimarães, V.; Lichtenthaler, R. et al. *Nucl. Phys. A* **2010**, *836*, 1–10.

[29] Satchler, G. R. *Direct Nuclear Reactions*; Oxford University Press: Oxford, UK, 1983.

[30] Thompson, I. J. *Comput. Phys. Rep.* **1988**, *7*, 167–212.

[31] Aygun, M. *Acta Phys. Pol. B* **2014**, *45*, 1875.

[32] Vineyard, M. F.; Cook, J.; Kemper, K. W.; Stephensens, M. N. *Phys. Rev. C* **1984**, *30*, 3.

[33] Reference Input Parameter Library (RIPL-3). Available online at https://www-nds.iaea.org/RIPL-3/.

[34] Nicoli, M. P.; Haas, F.; Freeman, R. M.; Szilner, S.; Basrak, Z.; Morsad, A.; Satchler, G. R.; Brandan, M. E. *Phys. Rev. C* **2000**, *61*, 034609.

[35] Koning, A. J.; Delaroche, J. P. *Nucl. Phys. A* **2003**, *713*, 231–310.

[36] Farag, M. Y. H .; Esmael, E. H.; Maridi, H. M. *Eur. Phys. J. A* **2014**, *50*, 106.

[37] Deshmukh, N. N.; Mukherjee, S.; Nayak, B. K.; Biswas, D. C.; Santra, S.; Mirgule, E. T.; Appannababu, S.; Patel, D.; Saxena, A.; Choudhury, R. K. et al. *Eur. Phys. J. A* **2011**, *47*, 118.